Fusion Engineering and Design 23 (1993) 201–217
North-Holland

Materials selection criteria and performance analysis for the TITAN-II reversed-field-pinch fusion power core

Shahram Sharafat [a], Nasr M. Ghoniem [a], Patrick I.H. Cooke [a,1], Rodger C. Martin [a,2], Farrokh Najmabadi [a], Kenneth R. Schultz [b], Clement P.C. Wong [b] and the TITAN Team *

[a] *Institute of Plasma and Fusion Research, University of California, Los Angeles, CA 90024-1597, USA*
[b] *General Atomics, San Diego, CA 92186, USA*

The TITAN-II reactor is a compact, high-neutron-wall-loading (18 MW/m^2) design. The TITAN-II fusion power core (FPC) is cooled by an aqueous lithium-salt solution that also acts as the breeder material. The use of an aqueous solution imposes special constraints on the selection of structural and breeder material because of corrosion concerns, hydrogen embrittlement, and radiolytic effects. In this paper, the materials engineering and design considerations for the TITAN-II FPC are presented. Material selection criteria, based on electrochemical corrosion mechanisms of aqueous solutions coupled with radiolysis of water by ionizing radiation, resulted in the choice of a low-activation ferritic steel as structural material for TITAN-II. Stress corrosion cracking, hydrogen embrittlement, and changes in the ductile-to-brittle transition temperature of ferritic alloys are discussed. Lithium-nitrate ($LiNO_3$) salt was chosen over lithium hydroxide (LiOH) because it is less corrosive and reduces the net radiolytic decomposition rate of the water. The dissolved salt in the coolant changes the thermophysical properties of the coolant results in trade-offs between the lithium concentration in the coolant, neutronics performance, thermal and structural design. The TITAN-II design requires a neutron multiplier to achieve an adequate tritium breeding ratio. Beryllium is the primary neutron multiplier, assuming a maximum swelling of about 10% based on continuous self-limiting microcracking/sintering cycles.

1. Introduction

The TITAN-II reactor is a compact, high-neutron-wall-loading (18 MW/m^2) design. An overview of the TITAN-II design is given in ref. [1]. The TITAN-II fusion power core (FPC) is cooled by an aqueous lithium-salt solution that also acts as the breeder material [2]. The major feature of the TITAN-II reactor is that the entire primary loop is located at the bottom of a low-temperature, atmospheric-pressure, pure-water pool. Detailed safety analyses show that the TITAN-II pool can contain the afterheat energy of the FPC and will remain at a low enough temperature so that tritium or other radioactive material in the primary coolant system will not be released.

The materials issues in an aqueous-solution-cooled fusion reactor are quite different from those of a liquid-lithium-cooled FPC such as the TITAN-I design [3]. The most significant differences between water-cooled and liquid-metal-cooled devices arise from the much higher coolant pressure in the water-cooled system, the electrochemical corrosion mechanisms of aqueous solutions, and the radiolysis of water by ionizing radiation. In the TITAN-II design, tritium breeding is accomplished in a lithium salt that is dissolved in the primary coolant (water). Concerns associated with water-cooled systems are further complicated by the addition of lithium salt to the water as it affects the corrosion mechanisms and radiolysis of the water. To this end, both lithium-hydroxide (LiOH) and lithium-nitrate ($LiNO_3$) salts were considered because of their high solubility in water. The $LiNO_3$ salt was selected as the reference salt material because: (1) $LiNO_3$ is less corrosive than LiOH, and (2) radiolytic decomposition

Present addresses:
[1] On assignment from Culham Laboratory. Abington, Oxfordshire, UK.
[2] Oak Ridge National Laboratory, Oak Ridge, TN 37831, USA.
* See p. 69 of this issue.

of water which results in the formation of highly corrosive substances is minimized when nitrate salts are added to water. Aspects of radiolysis of the TITAN-II coolant are discussed in Section 2.

The choice of aqueous lithium-salt solution as the primary coolant requires a structural material capable of withstanding the combined corrosive and irradiation environment of the FPC. Furthermore, one of the goals of the TITAN study has been to satisfy Class-C waste disposal criteria and achieve a Level-2 of safety assurance. A low-activation ferritic steel (alloy 9-C) was chosen over austenitic steels and over vanadium-base alloys. The structural material issues are discussed in Section 3. Hydrogen embrittlement, stress-corrosion cracking, and corrosion of ferrous alloys have always been major concerns and are therefore covered in some detail in Sections 4, 5, and 6, respectively. Included are also discussions related to the effects of the $LiNO_3$ salt solution on the various corrosion mechanisms.

The thermophysical properties of the aqueous solutions can be very different from those of pure water and are reviewed in Section 7. These changes can have significant effects on nuclear, thermal, and power-cycle performance.

The TITAN-II design requires a neutron multiplier to achieve an adequate tritium-breeding ratio. Beryllium is the primary neutron multiplier for the TITAN-II design. The anticipated behavior of beryllium is briefly discussed in Section 8. The effects of radiation on the TITAN-II primary insulating material, spinel ($MgAl_2O_4$), have been covered in detail in Ref. [3].

Section 9 gives a summary of the material engineering and design considerations of the TITAN-II design.

2. Radiolysis of aqueous solutions

Water and aqueous solutions undergo extensive radiolysis (i.e., chemical changes), when exposed to high levels of ionizing radiation (see ref. [4] for detailed discussions). Various products such as H_2 and H_2O_2 will form, depending on the composition, temperature, pH, and impurities present in the coolant. The radiolysis of water causes two major areas of concern. First, radiolysis can in principle create large quantities of explosive gas mixtures. Second, the radiolytic decomposition products, in particular H_2O_2, can enhance the corrosion rate of structural materials. It is desirable to quantify the radiolytic products as a function of water chemistry, impurity levels, temperature, and the characteristics of the radiation field. However, the complex interrelationship between environmental factors and the formation rates of the decomposition product makes this task very difficult. Furthermore, very little experimental data are available on production and recombination rates of radicals in aqueous $LiNO_3$ salt solutions. While the literature of the 1960s is rich in research performed on various nitrate solutions, $LiNO_3$ solutions specifically have only been studied during the last decade.

The TITAN-II FPC is cooled by an aqueous $LiNO_3$ salt solution. The presence of lithium atoms undergoing (n,α) reactions in the coolant introduces high-energy α and tritium recoil ions. These energetic ions, together with neutrons, interact with the surrounding water molecules causing the decomposition of water molecules. Contributions from both the ionizing radiation and the nuclear reactions in the aqueous solution have to be included in the analysis.

2.1. Molecular and radical yields in concentrated solutions

Reaction yield for a product, P, is denoted by $G(P)$ and refers to the number of radicals or molecules that are produced by radiation. Reaction yields are determined by chemical analysis and are expressed in terms of numbers of molecules or radicals produced per 100 eV of energy absorbed by the media. Reaction yields expressed in this manner do not represent the number of molecules or radicals that are produced directly by radiation, because these products decompose or interact further with other free radicals (yield of intermediate products is denoted by G_P).

Gamma rays – Over the past decade, considerable information has been accumulated on γ-ray yields in concentrated solutions, particularly for solutions containing nitrates such as $NaNO_3$, $LiNO_3$, $Ca(NO_3)_2$, and KNO_3. In order to explain radiolysis mechanisms of concentrated solutions, Kiwi and Daniels [5] progressively measured the yields of various nitrated solutions as a function of solute concentrations under γ irradiation. The radiolysis of nitrate solutions is characterized by a yield of nitrite ions (NO_2^-), increasing continuously with nitrate concentration up to the solubility limit, and the occurrence of O_2 as a major product. Kiwi and Daniels were able to explain and distinguish between the direct and indirect yields using an electron fraction model [6]. They concluded that for all of the nitrate solutions such as $NaNO_3$, $LiNO_3$, $Ca(NO_3)_2$, and KNO_3, and with more than 1 molar concentration, the major products are nitrite, peroxide, and oxygen. Table 1 lists the various yields as a func-

Table 1
Yields for gamma radiation in $LiNO_3$ solutions [a] [5]

Molarity [b]	H_2O_2	H_2	NO_2^-	O_2
1	0.63	0.15	1.4	0.35
2	0.53	0.09	1.5	0.75
3	0.45	0.05	~1.55	~0.8
5	0.35	0.03	~1.6	~0.85
7	0.33	< 0.01	~1.7	~0.6
9	0.26	< 0.01	~1.8	–

[a] In units of No./100 eV.
[b] Molarity, M, is defined in units of mol/liter of $LiNO_3$.

Table 2
Yields for $^6Li(n, \alpha)T$ reactions in $LiNO_3$ solution [a]

Molarity [b]	H_2	H_2O_2	H	OH	HO_2
0	1.2	1	0.7	0.4	0.2
2	1.08	0.9	0.57	0.32	0.15
3	1.00	0.85	0.53	0.31	0.14
5	0.95	0.79	0.50	0.28	0.13
7	0.90	0.75	0.47	0.27	0.13
9	0.86	0.72	0.45	0.26	0.12

[a] Yields (No./100 eV) are based on the power-law measurement by Burton [7].
[b] Molarity, M, is defined in units of mol/liter of $LiNO_3$.

tion of salt concentration in $LiNO_3$ solutions. Figure 1 shows that, as the molarity of the solution increases, $G(H_2O_2)$ and $G(H_2)$ decrease drastically. No yields for OH as a function of molarity were reported, since it was shown that G(OH) will be fairly independent of the concentration of the nitrate solutions [6]. Thus, for all practical purposes, the corresponding value for water can be used.

Alpha particles – While the γ-ray yields are well known as a function of $LiNO_3$ salt concentration, the α and tritium recoil yields have not been studied to this extent. However, Burton and Kurien [7] concluded that yields are more sensitive to the solute concentration when α-radiation was used compared to X rays. Table 2 shows the various yields as a function of salt concentration for radiation resulting from $^6Li(n,\alpha)T$ reactions.

Scavenging – For concentrated solutions, it is found that oxidizing agents will gradually decrease the H_2 yield as the concentration of the oxidant is increased,

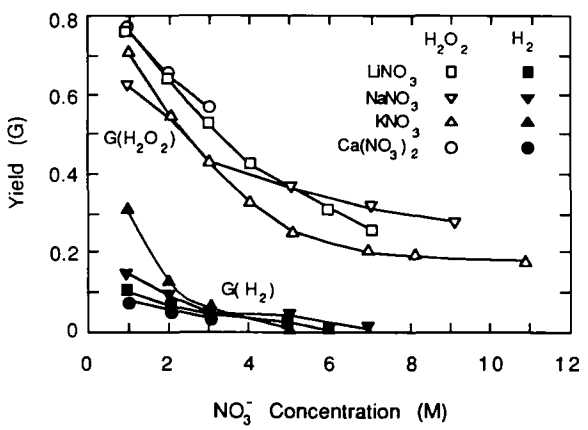

Fig. 1. Yields of hydrogen, $G(H_2)$, and hydrogen peroxide, $G(H_2O_2)$, as functions of molarity (mol/liter) of the nitrate salt solution.

and reducing agents will decrease the H_2O_2 yield [8]. This effect is expected, because solute molecules may react with the radicals before they have a chance to encounter a radical of the same kind. Thus, the probability of molecular product formation decreases as the solute concentration increases. The process of picking up and destroying radicals by solutes is referred to as "scavenging." Some experience has been gathered in the fission industry by using copper as a scavenger to reduce the molecular-product yield [9]. Schwarz [8] discovered that the hydrogen and peroxide yields could be greatly reduced by adding potassium nitrite or copper sulfate to the water. Nitrate ions at high concentrations were found to reduce the H_2 yield under nuclear reactor radiation to values less then 0.05 [10]. This result verified that molecular hydrogen does not form directly by splitting of the hydrogen from the water molecule, but by the combination of H atoms. Ferric ions are among other scavengers that reduce G_{H_2} in acid solutions [8]. In general, substances that react readily with H atoms reduce G_{H_2}, while those reacting with OH reduce $G_{H_2O_2}$. Thus, disolving $LiNO_3$ into the water coolant of TITAN-II is expected to decrease the yield of corrosive agents, in particular H_2O_2 and H_2 as demonstrated by the experimental data (see Table 1).

Temperature effects – In general, the stability of non-boiling water to radiolysis increases as temperature is increased, due to reaction rate increases between various radicals [11]. Most of the reported experimental data for nitrate solutions, do not include the effect of temperature on various yields. However, experiments in the High-Flux Irradiation Facility (HFIR) show a decrease of about an order of magnitude in yields for H_2 and H_2O_2, and about a factor of two decrease for HO_2 and O_2 yields as the temperature rises from room temperature to 200°C [12]. Similarly, it is expected that at elevated temperatures, yields of the

aqueous $LiNO_3$ coolant for TITAN-II will be less than present-day data reflect.

Tritium issues – The breeding of tritium in the coolant of TITAN-II will lead to the formation of HO_2 molecules. These molecules are precursors of free-oxygen formation (see Table 1). Experiments with power reactors have shown that if oxygen is added to the coolant at high power levels, rapid recombination with the existing hydrogen will occur [12]. Thus, although the aqueous solution containing $LiNO_3$ salt will produce more oxygen than the salt-free coolants of fission power reactors, the production of tritium should enhance oxygen-hydrogen recombination under non-boiling conditions. Furthermore, the nuclear reaction $^6Li(n,\alpha)T$ caused tritium atoms to recoil with 2.73 MeV of energy. Tritium atoms have been shown to react chemically while still possessing some of the kinetic energy. The high-energy tritium, "hot hydrogen," is believed to undergo a hydrogen abstraction reaction, while thermal hydrogen interacts mostly with existing radicals. Kambara et al. [13] have made a detailed study of the HT:HTO ratio formed during neutron irradiation of various lithium-containing solutions. They studied aqueous solutions of $LiNO_3$, LiOH, and LiCl at pH values ranging from 1 to 11 irradiated to a total flux of 10^{14} to 10^{15} neutrons/cm^2. They found all HT:HTO ratios fall in the range of 0.04 to 0.12 with an average ratio of 0.10 ± 0.01. Table 3 shows the HT:HTO ratios of some of the solutions studied. The choice of lithium salt does not significantly affect the HT:HTO ratio.

Table 3
HT:HTO ratios of neutron-irradiated solutions [13]

Solution	HT:HTO ratio
1.5 *M* $LiNO_3$, 0.1 *M* NaOH	0.06
1.5 *M* $LiNO_3$, 0.1 *M* NaOH	0.08
0.6 *M* LiOH	0.04
0.7 *M* LiCl, pH 14	0.048
1.0 *M* LiCl, 1 *M* NaOH	0.07

In summary, radiolysis of aqueous $LiNO_3$ salt solutions by light and heavy particles was investigated. Gamma-ray radiolysis yields of $LiNO_3$ salt solutions are known as a function of salt concentration. At high concentrations, the H_2 yields are very small and the H_2O_2 yield decreases by a factor of about 3 relative to pure water. Oxygen yields of light-particle radiation are fairly independent of the salt concentration. Energetic α particles (3.4 MeV) are produced by nuclear reactions with lithium in the aqueous $LiNO_3$ salt solution. Reaction yields were estimated as a function of salt concentration based on the power-law measurements of 3.4-MeV α particles. The oxygen production by heavy-particle radiation increases while the yields of H_2, H_2O_2, H, OH, and HO_2 all decrease with increasing salt concentration. The increase in oxygen production due to radiolysis may be balanced by the production of tritium atoms. It has been shown that oxygen added to non-boiling fission-reactor coolants at high power levels rapidly combines with any hydrogen pre-

Table 4
Physical and mechanical properties of alloy 9-C low-activation ferritic steel [14]

Property	Temperature (°C)				
	RT	300	400	500	600
Young's modulus (GPa)	225	200	193	180	150
Poisson ratio	0.4	0.4	0.4	0.4	0.4
Shear modulus (GPA) [a]	83	75	72	68	–
Tensile strength (MPa)	1002	–	810 [a]	942 [b]	749 [c]
Yield strength (MPa) [c]	810	810	820	650	531
Total elongation (%) [c]	10.1	13.8	15.0	17.0	19.4
Thermal-expansion coefficient (10^{-6}/°C)	9.5	10.5	11.0	11.5	12.0
Specific heat (J/kg-°C)	450	570	600	680	780
Electric resistivity ($\mu\Omega$ m)	0.6	0.82	0.9	0.99	1.05
Thermal conductivity (W/m-K)	25	26.5	26.7	27.2	27.6
DBTT at 15 dpa (°C) [a]	–	–	100	25	0
DBTT at 30 dpa (°C) [a]	–	–	140	50	55

[a] Data unavailable, corresponding values for HT-9 were used.
[b] Values at irradiation temperatures after 6 dpa.
[c] Values at irradiation temperatures after 14 dpa.

sent. The decrease in the yield of free radicals in concentrated $LiNO_3$ solutions makes this salt more favored than LiOH solutions. The effect of elevated temperature on radiolysis was investigated. From experience gained in the fission industry with pure water, it can be ascertained that the stability of the TITAN-II non-boiling aqueous $LiNO_3$ solution to radiolysis increases as temperature increases.

Although many uncertainties remain and much research is required in the area of radiolysis, the use of a highly concentrated, aqueous $LiNO_3$ salt solution should not lead to the formation of volatile or explosive gas mixtures. The effects of radiolytic decomposition products on corrosion, however, remain uncertain and experimental data on the behavior of radiolytic decomposition products in a fusion environment are needed.

3. Structural material

Irradiation of commercial steels in a fusion environment produces long-lived radioactive isotopes. Effort has been made to develop low-activation alloys by replacing those alloying elements that would not qualify for Class-C waste disposal with more suitable ones, without compromising mechanical properties. As a result, reduced-activation-alloys (sometimes referred to as low-activation ferritic steels) have been produced. One approach has been to replace molybdenum with vanadium rather than with tungsten [14]. To avoid delta-ferrite formation, manganese is added to the high-chromium alloys and carbon contents are kept very low (< 0.1 wt%). To compensate for the effects of carbon as a solute strengthener, the manganese content had to be increased substantially ($\sim 6.5\%$ Mn). Compared with $2\frac{1}{4}$Cr–1Mo, the low-chromium bainitic alloy ($2\frac{1}{4}$Cr–V) has a lower yield strength, a slightly lower ultimate tensile strength, and a much higher elongation [15]. On the other hand, the 12-Cr martensitic alloys show a higher strength with comparable elongation when compared with commercial 12Cr–1Mo–V–W steels [15]. Table 4 shows selected properties of the 9-C alloy. The composition (wt%) of the 9-C alloy was determined by the vendor as: 11.81Cr, 0.097C, 0.28V, 0.89W, 6.47Mn, 0.11Si, 0.003N, < 0.005P, and 0.005 with balance in iron.

The effects of irradiation on the low- and high-chromium alloys were also investigated [14] and the latter were found to be superior. Under irradiation, the $2\frac{1}{4}$Cr–V alloys showed an increase in strength and a reduction in elongation, while the 9 to 12Cr–Mn–V–W

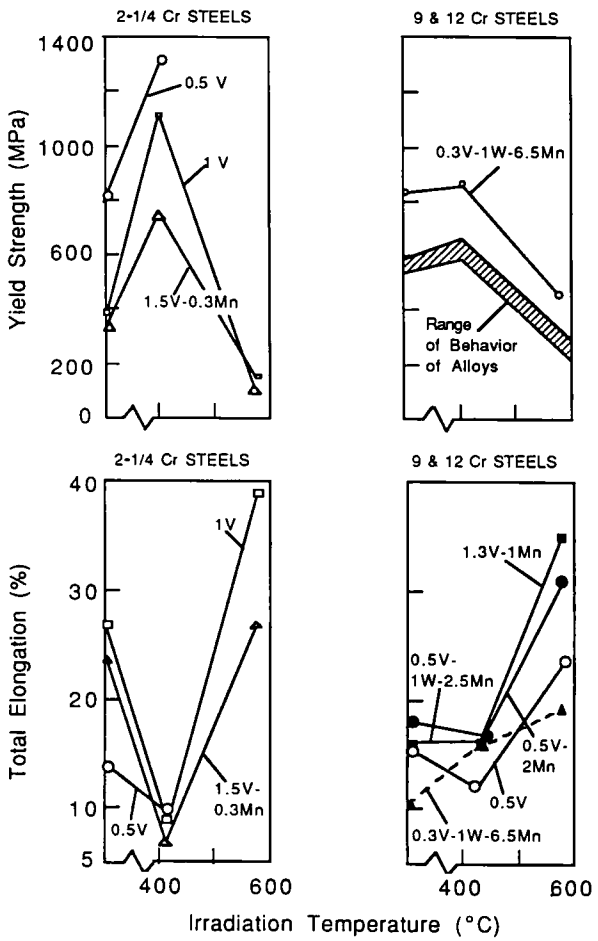

Fig. 2. Results of uniaxial-tensile tests of HEDL low-activation ferritic alloys [15]. The yield strength and the total elongation are plotted as a function of the irradiation temperature. The values on the vertical axis denote the corresponding values for an unirradiated specimen.

alloys exhibited only small changes in strength and elongation after irradiation at 420°C and damage doses up to 10 dpa [14]. The radiation-hardening resistance of high-chromium alloys is also significantly different from commercial high-chromium ferritic steels such as 9Cr–1Mo–V–Nb and 12Cr–1Mo–V–W (HT-9) [15,16].

Some data on irradiation behavior of the low-activation ferritic steels are available. Specimens were irradiated up to 14 dpa in the FFTF and post-irradiation tests were performed at room temperature. Figure 2 shows a comparison of the yield strength and total elongation of low-activation ferritic steels as a function of irradiation temperature (values on the vertical axis

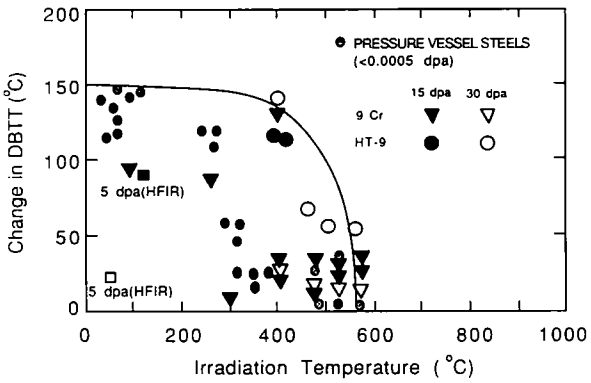

Fig. 3. Change in the DBTT as a function of irradiation temperature for 9Cr–1Mo–W–Nb and HT-9 ferritic steels [17].

corresponding to the unirradiated specimen). It can be seen that $2\frac{1}{4}$Cr–V alloys experience an increase in strength of about 200 MPa when irradiated at 420°C. At 585°C, however, these alloys show a reduction of strength compared with unirradiated alloys. The high-chromium alloys show much smaller irradiation-hardening effects at 420°C. A reduction in strength at 585°C is also experienced by the high-chromium alloys, but the decrease is not as much as that of the low-chromium alloys. The 12Cr–0.3V–1W–6.5 Mn martensitic steel shows the smallest degree of irradiation hardening and the lowest decrease in strength of all tested alloys. Figure 2 also shows the total elongation of the tested specimen. Again 12Cr–0.3V–1W–6.5Mn martensitic steel shows the smallest fluctuations in total elongation among all tested alloys.

The ductile-to-brittle transition temperature (DBTT) of some ferritic alloys may be a potential problem. The DBTT is the temperature at which the fracture stress is reached during loading of a specimen prior to the onset of the yield. When a specimen is loaded at a temperature below the DBTT, a brittle-type cleavage fracture occurs, while at temperatures above the DBTT the metal undergoes yielding before fracture occurs. Figure 3 shows changes in DBTT of 9Cr–1Mo–W–Nb and 12Cr–1Mo–W–V (HT-9) irradiated to damage levels of up to 30 dpa as a function of irradiation temperature. The change in DBTT is highest at low irradiation temperatures, and vanishes when irradiation temperatures exceed 600°C. The commercial 9-Cr alloy shows smaller increases overall in DBTT when compared with HT-9. Recently, Lechtenberg [17] investigated the DBTT of the reduced-activation 9Cr–2W–0.15C stabilized martensitic steel. The DBTT of the unirradiated specimen was −24°C. When irradiated at 356°C to damage dose of 10.5 dpa, the DBTT increased to about 0°C. The measured increase on DBTT of 24°C is the smallest increase reported among all the low-activation ferritic alloys studied. The DBTT of tested ferritics clearly indicates a potential problem. Until alloy-development efforts alleviate this problem, operating conditions must be chosen to minimize the rise in DBTT of ferritic steels.

In summary, among the low-activation candidate vanadium alloys, V–3Ti–1Si had to be ruled out because of its poor water-corrosion resistance. Other vanadium alloys that contain chromium (e.g., V–15Cr–5Ti) show excellent resistance to corrosion by water coolant but their properties are inferior to those of ferritic steels when helium-embrittlement effects are taken into account [18]. The 12Cr–0.3V–1W–6.5 Mn alloy (9-C) has been chosen as the structural material, primarily because of its high strength and good elongation behavior after irradiation as compared with other low-activation ferritic steels. The high-chromium content of this alloy ensures an excellent corrosion resistance, while the low carbon content of this alloy results in good weldability, high sensitization resistance, and a reduction of hydrogen-embrittlement susceptibility. Furthermore, alloy 9-C has a low tungsten content ($< 0.9\%$) which reduces the waste-disposal concerns of the production of the radionuclide ^{186m}Re by fusion-neutron reaction with W. The high concentration of manganese in 9-C prevents the formation of delta-ferrite phases, which is responsible for high DBTT and low hardness.

4. Hydrogen embrittlement

Hydrogen embrittlement is caused primarily by atomic, diffusible, or nascent hydrogen (H) content, and not by the total hydrogen content that may also include molecular hydrogen (H_2). Much confusion exists in the relationship between stress-corrosion cracking (SCC) and hydrogen embrittlement because the crack-growth mechanism of both processes is the same. For SCC to occur, the crack has to be in contact with the aqueous solution. During corrosion processes in aqueous solutions, atomic hydrogen is generated which is absorbed by the crack tip. Stress-corrosion cracking is, therefore, a special case of hydrogen embrittlement in which hydrogen is produced by the corrosion process occurring inside the crack (see ref. [4] for detailed discussion).

4.1. Hydrogen embrittlement of ferrous alloys

The primary factors that affect the behavior of ferrous alloys in a hydrogen-bearing environment are: (1) hydrogen concentration, (2) temperature, (3) heat treatment, (4) microstructure, (5) stress level, and (6) environment. The tendency for hydrogen embrittlement to occur increases with hydrogen concentration in the metal, resulting in reduction of the time-to-failure and the stress levels at which failure occurs [19]. The effects of various elements on hydrogen embrittlement have also been studied in great detail. In general, elements such as carbon, phosphorus, sulfur, manganese, and chromium increase the susceptibility of low-alloy steels to hydrogen embrittlement. The susceptibility of stainless steels to hydrogen embrittlement can be directly related to its strength. Stainless steels can have very low resistance to hydrogen embrittlement with increasing yield strength when exposed to aqueous or gaseous hydrogen [20]. Generally, the threshold stress intensity for crack growth decreases with increasing yield strength. The reason for this stress behavior is not entirely clear but it has been related to a change in hydrogen-assisted failure modes, with blistering becoming the dominant failure mechanism for low-strength steels.

Ferritic steels show an excellent resistance to hydrogen embrittlement because of their enhanced ductility and lower strength characteristics [21]. By examining a wide range of ferritic alloys that had undergone different heat treatments, Bond et al. [21] concluded that ferritic steels can be embrittled only after severe and extensive hydrogen charging from aqueous solutions. Furthermore, they concluded that cracking is intensified by welding, high-temperature heat treatment, and cold working. The chemical composition of the alloys was found to be less important under conditions of hydrogen charging.

The effects of temperature on hydrogen embrittlement have been investigated in detail. Hydrogen embrittlement has been observed in ferrous alloys over a wide range of temperatures, $-100°$ to $+700°C$. However, the most severe embrittlement in steels occurs around room temperature [22–25]. The temperature dependence of the tensile strength of a high-strength steel is shown in Fig. 4. At very low ($-100°C$) or very high (700°C) temperatures, the tensile strength of a hydrogen-charged steel approaches the values of a hydrogen-free sample [26]. This temperature dependence can be explained by noting that at high temperatures, thermal agitation may cause de-trapping of a hydrogen atom which will then diffuse rapidly through the matrix. The combination of these two effects, a higher de-trapping rate and a higher mobility, results in a low hydrogen concentration at high temperatures. At very low temperatures, on the other hand, the diffusivity of hydrogen atoms is reduced to such a small value that trap sites would not be filled.

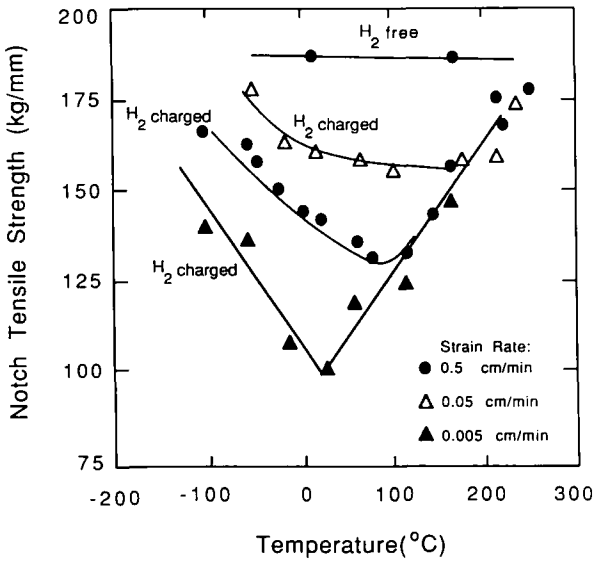

Fig. 4. Tensile strength of a high-strength steel as a function of testing temperature for three strain rates [26].

Figure 4 also shows that hydrogen embrittlement is highly sensitive to the strain rate. At a very high strain rate, the cracking proceeds without the assistance of hydrogen. The hydrogen mobility is not sufficient to maintain a hydrogen atom cloud around the moving dislocations. At a low strain rate, crack propagation is slow enough to keep the hydrogen concentration around the moving dislocations at levels that influence cracking. Cracking that is influenced by the presence of hydrogen falls into the category of stress-corrosion cracking.

4.2. Hydrogen-embrittlement prevention

Techniques for in-service hydrogen-embrittlement prevention generally focus on either eliminating the source of hydrogen or minimizing stresses to below the threshold values necessary to cause cracks. For nuclear components, however, the hydrogen source from (n,p) reactions can never be totally eliminated. Nevertheless, hydrogen embrittlement may be mitigated or prevented by application of one or more of the following preventive measures (see ref. [4] for more detail): (1) reducing

corrosion rates by water chemistry control, (2) baking or removal of hydrogen from the metal before damage has occurred, (3) alloy selection and tailoring, (4) reduction of SCC by deaeration (removal of oxygen by adding H_2) of boiler water.

Experiments with the addition of hydrogen to water in BWRs has shown that SCC and corrosion can be reduced markedly [27–31]. These experiments demonstrate the different effects between nascent (monatomic, adsorbed, and diffusible) hydrogen and molecular (H_2) hydrogen. While nascent hydrogen increases SCC, molecular hydrogen decreases SCC because of recombination with dissolved oxygen.

Petrochemical plants expose metals to high temperatures and high hydrogen pressures (hydrogenation processes). The dissociation of molecular hydrogen under conditions of high pressure and high temperature is a major source of diffusible hydrogen. The reaction of hydrogen with carbon has been identified as the main cause of hydrogen embrittlement in hydrogenation processes. The petrochemical industry has adopted a practical solution to this problem by using low-alloy steels. These steels contain carbon stabilizers such as chromium, molybdenum, tungsten, vanadium, titanium, and niobium. In addition to altering the microstructure of the alloy, these alloying elements also reduce the reactivity of carbon with absorbed hydrogen. Experience in the petrochemical industry has resulted in the development of "Nelson curves" [32] which prescribe the acceptable limits of temperature and hydrogen partial pressure for common low-alloy steels. An example of these curves is shown in Fig. 5. It can be seen that a higher chromium content allows higher temperatures and higher hydrogen partial pressures. The worst case is that of regular carbon steel.

In summary, hydrogen embrittlement is an important phenomena caused mainly by the trapping of absorbed hydrogen in metals under applied stresses. The main factor influencing hydrogen embrittlement is the hydrogen content, and that depends strongly on the temperature, microstructure, and strength of the alloy. Hydrogen content can be reduced by minimizing the source of nascent hydrogen (mostly made available through corrosion processes) and by operating at high temperatures (> 200°C), provided that a low-carbon steel is used. High concentrations of chromium, nickel, or molybdenum (> 10 wt%) increase the resistance of ferrous alloys to hydrogen damage. Microstructural features such as a fine-grained and annealed alloys with minimum cold work further reduce susceptibility to hydrogen embrittlement. Because of the lower strength and higher ductility of ferritic steels, these

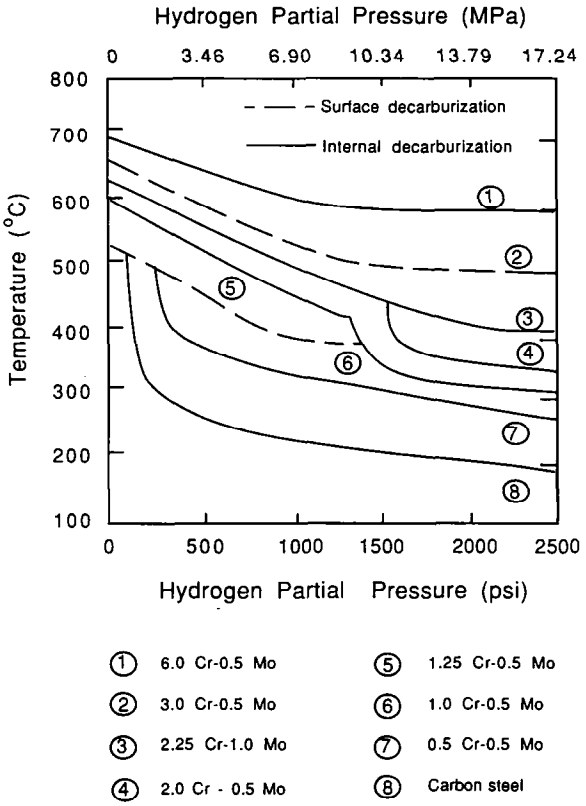

Fig. 5. Operating limits (Nelson curves) for steels in hydrogen service [33].

alloys are generally less susceptible to hydrogen embrittlement than austenitic steels.

The production of hydrogen by nuclear reactions and by plasma-driven permeation through the first wall of a fusion device increases the hydrogen content inside the alloy matrix which may lead to unacceptable hydrogen embrittlement of the structure for operation at or near room temperature (the condition of highest susceptibility [33]). But the TITAN-II structural material operates at high temperatures (> 400°C), minimizing the effective trapping of hydrogen inside the matrix. Experiments show that above ~ 200°C, hydrogen embrittlement of ferrous alloys is reduced markedly [34]. Furthermore, the Nelson curves indicate that 2.0 Cr-0.5 Mo steel can operate at 400°C with a hydrogen partial pressure of 17 MPa without internal decarburization and hydrogen embrittlement (Fig. 5).

Based on the above discussion, the ferritic alloy 9-C is expected to exhibit a high resistance to hydrogen embrittlement. The number of factors influencing hydrogen embrittlement are numerous and their interde-

pendence is a complex function of the specific microstructure and operating conditions of an alloy. Therefore, experimental data are needed in order to perform a complete evaluation of hydrogen embrittlement of the 9-C alloy under TITAN-II operating conditions.

5. Stress-corrosion cracking (SCC)

Major corrosion-related problems encountered by the utility industry and nuclear-steam-system suppliers include the intergranular stress-corrosion cracking (IGSCC) of welded austenitic stainless-steel pipes in boiling-water reactors (BWRs) and the steam-generator corrosion in the pressurized-water reactors (PWRs) [35]. Despite the differences in operating conditions and coolant environments, the primary materials problem for both BWRs and PWRs is SCC. During SCC, a metal is virtually unattacked over most of its surface while fine cracks progress through the bulk of the material. The alloy becomes brittle with little or no macroscopic plastic deformation. Stress-corrosion cracking can occur both in transgranular (across grains) or intergranular (between grains) modes. Intergranular stress-corrosion cracking (IGSCC) is found to be the dominant failure mechanism in sensitized austenitic stainless steels, while transgranular SCC (TGSCC) has been reported to occur primarily in ferritic and low-alloy steels [28]. Three requirements must be fulfilled simultaneously for SCC to occur: (1) the steel must be sensitized, (2) the steel has to be under tensile stress, and (3) the environment must have specific corrosion properties (e.g., excess oxygen).

Ljungberg et al. [28] tested 20 different steels including ferritic steels. Their results indicate that ferritic steels are sensitive to TGSCC under pure-water conditions (PWC). However, with hydrogenated water (alternate-water conditions, AWC), no TGSCC was observed (oxygen contents < 10 ppb). They concluded that TGSCC in ferritic and martensitic steels may be inhibited at a somewhat greater oxygen content in the reactor water than that needed for inhibiting IGSCC in sensitized stainless steel.

The fact that the AWC mitigates TGSCC in ferritic and martensitic steels with a somewhat broader margin of acceptable oxygen levels than for IGSCC in sensitized austenitic steels was also observed and reported by DRESDEN-2 experimentalists [30]. It should be noted that TGSCC of the type measured in the above-mentioned experiments has never occurred in an operating BWR. Presumably it is specific to the extreme mechanical conditions prevailing in the tests, with a constant extension rate such as the TGSCC observed in austenitic stainless steel with AWC.

Gordon et al. [31] also investigated the corrosion resistance of ferritic steels through hydrogen addition to BWR coolants. At a test temperature of 288°C, the oxygen content was held close to 20 ppb by dissolving 125 ± 25 ppb hydrogen at a pressure of 8.69 MPa. Low-alloy and carbon-steel samples were characterized by no crack growth under constant load-stress intensities of up to 50.9 MPa-$m^{1/2}$. Under cyclic loads, these samples showed a 7 to 20 times lower crack-propagation rate compared with samples exposed to nominal BWR environment (200 ppb oxygen). Furthermore, the addition of hydrogen to the test water did not show any evidence of hydrogen stress cracking or hydrogen embrittlement in low-alloy and high-strength, wrought martensitic stainless steels.

In addition to the control of the water chemistry, another remedy to SCC has been to develop alternative SCC-resistant materials. The most important materials of this type are the nuclear-grade stainless steels such as AISI 304NG and 316NG. These steels have a low carbon content (0.2 wt%) to avoid sensitization, but contain nitrogen (between 0.06 and 0.1 wt%) to maintain the strength required by the ASME Boiler and Pressure Vessel Code. These nuclear-grade materials have been found to be much more IGSCC resistant than the regular AISI 304 and 316 stainless steels [36].

In summary, a reduction of oxygen content through the addition of hydrogen to the coolant can reduce SCC in most ferritic and austenitic alloys. Also alloying elements significantly affect SCC. The high chromium content of the 9-C alloy (11.84 wt%) is very helpful in reducing the susceptibility of this alloy to SCC. The carbon content of the 9-C alloy (0.097 wt%) is outside the range of highest SCC susceptibility but is high enough for sensitization to occur (> 0.02 wt%) if the alloy is heated to temperatures above ~ 950°C.

6. Corrosion in nitrates

Because corrosion is primarily an electrochemical process, the electromagnetic environment of a fusion device can have unforeseen effects on the corrosion rates by the aqueous solutions. The complexity of various environmental factors such as temperature, velocity, oxidizers, and other impurities have to be considered in assessing corrosion processes [4]. The interdependence of these environmental factors is too great to

allow any decisive conclusions regarding approximate corrosion rates. Lack of knowledge of the effects of irradiation and the effects of radiolytic decomposition products on corrosion mechanisms will undoubtedly further complicate the understanding and extrapolation of existing data.

Experience with various aqueous nitrate-salt solutions shows that the choice of the cation will affect the degree of corrosion attack. The aggressiveness of nitrates decreases with choice of the cation in the following order: NH_4, Ca, Li, K, and Na [37]. Thus for the $LiNO_3$ salt, the aggressiveness of NO_3^- ions is in the medium range. Recent experiments [38] on the corrosion rates of $LiNO_3$ salt solutions with 316 SS and with a martensitic alloy at 95° and 250°C imply that a relatively stable passive layer is formed in this salt. Microscopic examination of the 316 SS showed that a smooth oxide film was formed on the metal surface in $LiNO_3$, with the roughness independent of solution concentration and temperature. Recently, electrochemical corrosion tests were performed for aqueous LiOH and $LiNO_3$ solutions in contact with AISI 316L stainless steel [39]. It was found that stainless steels, particularly low-carbon steels, exhibit better corrosion resistance in an $LiNO_3$ solution than in LiOH.

It should be noted that most of the experimental findings regarding corrosion and SCC of steels in $LiNO_3$ salt solutions were obtained without any control of the oxygen content of the solution which plays a significant role. In a fusion environment, the production of tritium will undoubtedly affect the oxygen content of the aqueous solution through recombination. Thus, breeding of tritium in the aqueous solution can potentially reduce corrosion and SCC of the structural material used in the FPC.

The investigation of the corrosion of ferritic steels in an aqueous $LiNO_3$ salt solution does not show unexpectedly high corrosion rates or high susceptibility to SCC [37–44]. In addition, the latest experimental findings do not indicate any unforeseen catastrophic corrosion attack. However, an extensive research effort needs to be undertaken to confirm these observations.

7. Properties of $LiNO_3$ solutions

The physical properties of concentrated solutions of $LiNO_3$ at high temperatures differ from those of pure water. Therefore, a fairly detailed investigation of the physical properties of the aqueous solutions was made, including an extensive literature survey, to ensure that reliable data were used in analyzing the performance of the TITAN-II FPC. The physical properties of $LiNO_3$ solutions as functions of temperature and salt concentration are briefly discussed here with more detail given in ref. [4].

In many cases, experimental data for some physical properties of interest for $LiNO_3$ solutions are not available at high temperatures. Where this is the case, and reasonable extrapolations cannot be made, the corresponding data for NaCl solutions have been used because the $NaCl–H_2O$ system has been much more widely studied than any other solution and many solutions of 1–1 electrolytes (e.g., NaCl, KBr, and $LiNO_3$) have similar properties at the same concentrations. It is expected that such estimates should be accurate to about 20% [45], which is adequate for a worthwhile assessment of the thermal performance of the blanket.

Density – A full experimental data set is available for the density of $LiNO_3$ solutions for temperatures up to 350°C and for concentrations from pure water to pure $LiNO_3$ [46,47]. In ref. [46], an expression is fitted to experimental data for weight percentages up to 40% and for temperatures up to 300°C, the fit being accurate to better than 1.5% throughout the range. In ref. [47], experimental data are given for weight percentages from 40% to 100% $LiNO_3$ and for temperatures up to 350°C. To yield a smooth set of data over the entire range of temperatures and compositions under consideration, the fit [46] has been used for the lower concentrations and the experimental data for the higher concentrations, with the data being slightly smoothed in the transition range between the two data sets. Figure 6 shows the density as a function of temperature for various values of the lithium-atom percentage. This figure shows that for the higher concentrations, density is significantly increased from the pure-water value, the difference being a factor of about two for a lithium-atom content of 8%. A final point arising from these papers is that the authors note that $LiNO_3$ and H_2O are completely miscible at temperatures above the melting point of $LiNO_3$ (253°C). This implies that there is effectively no upper limit to the salt concentration for high temperatures from solubility considerations.

Viscosity – References [48,49] give experimental results for the viscosity of $LiNO_3$ solutions for temperatures up to 275°C and for concentrations up to 10 mol/kg (~ 4.5% Li), and provide fits to these data. They quote a fit to the viscosity of the solution relative to that of pure water, according to which there is about a factor of 6 increase in the viscosity of the 8% $LiNO_3$ solution compared with that of pure water. This large change can have a significant effect on the thermal

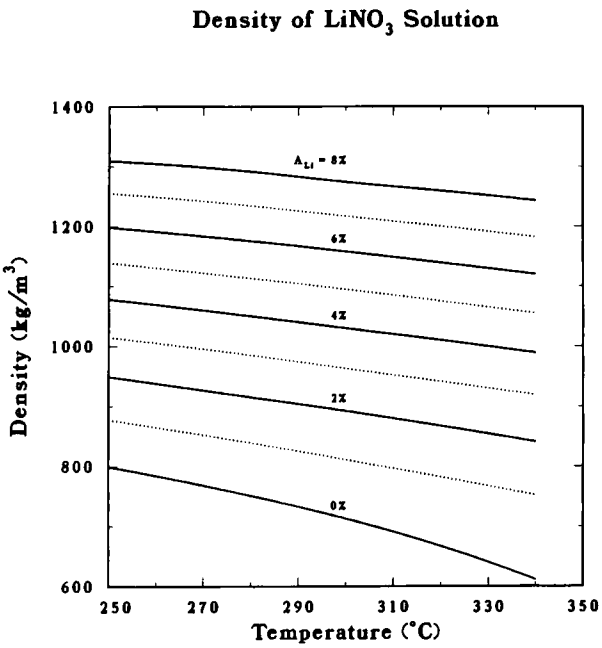

Fig. 6. Density of $LiNO_3$ solutions at various temperatures and for a range of lithium-atom percentages.

performance of the coolant, although some of the change is reduced by differences in other properties. As the data fit has been used well outside its quoted range of validity, it is important to recognize that there is a large degree of uncertainty associated with these values. However, the general trend in the values should be correct and, until better experimental data become available, it is reasonable to use these estimates to assess the potential of $LiNO_3$ solutions as fusion-blanket coolants.

Specific heat capacity – The specific heat capacity is a more difficult quantity to predict using a polynomial-type equation or by simply relating it to the value for pure water at the same temperature. The difficulty arises because the specific heat capacity of pure water becomes infinite as the critical point (374°C and 22.1 MPa) is approached. The addition of even small quantities of a salt changes the critical temperature and pressure quite significantly. Therefore, the specific heat capacity of the solution can vary markedly from that of pure water at the same conditions. Wood and Quint have proposed a very simple way of estimating the specific heat capacity for aqueous salt solutions using a "corresponding-states" method [50]. In this method, the properties of the solution are approximated by the properties of water at the same "relative" conditions with respect to the critical point.

In order to use this method to estimate the specific heat capacity for $LiNO_3$ solutions, the critical temperature and pressure of the solution must be known as a function of concentration. No measurements for $LiNO_3$ salt appear to have been made, but data are available for many other salt solutions [51] and it has been found that many 1–1 electrolytes have very similar critical temperatures at the same molality. Since an extensive data set is available for NaCl [52], these data have been used as a reasonable approximation for $LiNO_3$, although a large extrapolation has been made from the highest NaCl concentrations studied (6 mol/kg) to the most concentrated $LiNO_3$ solutions proposed. The data of estimated critical temperature and pressure for $LiNO_3$ solutions have then been used to yield specific heat capacities of the aqueous salt solution. These data were evaluated for a pressure of 10 MPa, but the specific heat capacity varies by less than 1% for pressures up to 16 MPa, except for the case of pure water.

Thermal conductivity – There appear to be no extensive experimental measurements of the thermal conductivity of $LiNO_3$ solutions for the temperature range of interest for fusion blankets. Data for NaCl are available, however, and ref. [53] gives smoothed values of experimental data for temperatures up to 330°C and for concentrations up to 5 mol/kg. These data were extrapolated to 11 mol/kg ($A_{Li} \sim 5\%$) and a simple fit to the data was made. For higher concentrations, curve fits were used as the simple fit breaks down. The estimates suggest that the difference in the thermal conductivity of the solution compared with that of pure water is not as marked as for other properties. However, as the original NaCl data are not precise, and these results have been extrapolated to higher concentrations and applied to $LiNO_3$ solutions. Further experimental data are required for a more exact assessment of the thermal performance of the coolant.

Boiling point – Reference [54] reported measurements of the vapor pressure of $LiNO_3$ solutions for concentrations up to 24 mol/kg and for temperatures up to 110°C. Their results showed that the relative vapor pressure (the ratio of the vapor pressure of the solution to that of pure water) for a given concentration remained approximately constant, independent of changes in temperature. In the absence of relevant experimental data, it has been assumed that this relationship is valid for higher temperatures. The boiling point of the solution is then evaluated by finding the temperature at which the vapor pressure is equal to the applied pressure. Figure 7 shows these results for

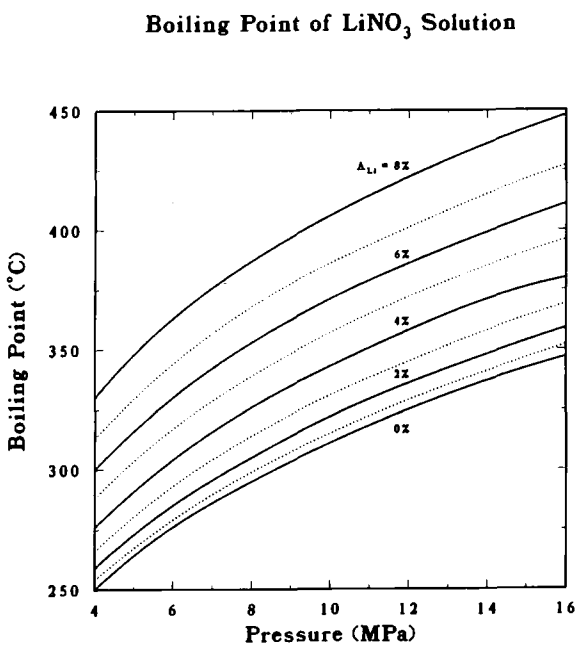

Fig. 7. Boiling temperatures of $LiNO_3$ solutions at various pressures and for a range of lithium-atom percentages.

pressures ranging from 4 to 16 MPa. These estimates of the boiling point indicate that the boiling point of the $LiNO_3$ solution should be significantly higher than of pure water. For a lithium-atom percentage of 5%, the increase is 40° to 50°C, which has a major effect on the thermal design of the fusion blanket. Once again, a note of caution is necessary because the accuracy of these estimates is uncertain since an extrapolation was made from the lower temperature results.

In summary, the above estimates of the properties of $LiNO_3$ solutions at high temperatures exhibit marked differences from the properties of pure water. Therefore, the exact coolant conditions should be considered in designing the blanket. The thermal-hydraulic design of an aqueous salt blanket can be very different from that of a water-cooled design, and advantage can be taken of the differences in properties by, for example, reducing the coolant pressure or increasing the temperature without incurring an increased risk of burnout. However, many of the estimates are extrapolations from experimental data or have been obtained from the results for other salt solutions. Although these predictions should give good indications of the expected trends for the various properties, a much expanded experimental data base is required for the salts and conditions proposed before the thermal performance of an aqueous salt blanket at high temperature can be confidently predicted.

8. Neutron-mutiplier material

Beryllium is chosen as the neutron-multiplier material for the TITAN-II design mainly because of low activation. Concerns associated with the beryllium choice for the TITAN-II design are water-corrosion behavior and radiation damage response which are discussed here (for details see ref. [4]).

Beryllium corrosion – Beryllium that is clean and free of surface impurities (in particular chlorates and sulfates) has exceedingly good resistance to attack in low-temperature, high-purity water [55], with typical corrosion rates of less than 1 mil/y [56]. In a slightly acidic demineralized water of a nuclear test reactor, beryllium has performed without problems for over 10 years [57,58]. Beryllium exposed to chloride and sulfate-contaminated aqueous solutions is susceptible to attack. Development of corrosion-protective coatings for beryllium has been extensive [57]. Extremely thin (100 Å) chromate coatings produced by simple dip treatments have shown to hold up under 5% salt spray tests for a period of 120 h [59]. With anodized coatings, no corrosion was detected after 2000-h exposure in ASTM salt-spray tests [57]. Uniform and adherent anodized coatings on Be are produced either by solutions of 50% HNO_3 with a current density of 0.20 A/ft^2 for 5 minutes, or by solutions of 7.5% NaOH with a current density of 10 A/ft^2 for 20 minutes. It is conceivable to develop an in-situ anodizing mechanism to coat Be in an aqueous self-cooled blanket. In particular, the TITAN-II blanket coolant contains both NO_3 and OH ions. Extensive research into this area will be required to establish the feasibility of in-situ anodizing methods.

For TITAN-II, the Be will be clad in the low-activation ferritic steel alloy, 9-C. Allowance must be made in the cladding-gap design to accommodate the anticipated swelling of Be and for encapsulating released helium gases. However, in the event of cladding failure, the above discussion indicates that control of coolant chemistry (minimizing carbonates and sulfates) will ensure low Be corrosion rates.

Swelling – A major concern associated with Be in a fusion environment is irradiation-induced swelling, which is mostly caused by helium-gas generation from (n, α) reactions. Helium atoms are insoluble in metals and consequently they will rapidly diffuse through the metal until they become immobilized at trap sites such

as thermodynamically and irradiation-produced dislocations, cavities, and grain boundaries. This phenomena is responsible for the nucleation and growth of bubbles. At high temperatures (above 700°C), bubbles can also migrate through the matrix or along grain boundaries and coalesce to form bigger bubbles (increased swelling).

The threshold temperature below which swelling of Be is insignificant was determined in early post-irradiation experiments [60–63]. For fluences resulting in a few appm of helium-atom concentration in Be, the threshold temperature is around 700°C while for fluences creating more than 50 appm of He, swelling threshold temperature drops to about 500°C. Beryllium located behind the first wall of a fusion device will have a helium generation rate of about 10,000 He appm/1 MW y-m^2. Because of these high helium-generation rates, suppression of Be swelling through operation at low temperatures is not feasible in a fusion blanket.

High-temperature (1000°C), post-irradiation anneal experiments showed a maximum swelling of 30%. This swelling maximum was attributed to interconnecting bubbles that resulted in a release of trapped He from the bulk. The minimum swelling necessary to produce an interconnecting network of He bubbles for gas venting was theoretically determined to be 5% to 10% [64]. Thus, Be exposed to high levels of fast-neutron irradiation will swell a minimum of about 10% and a maximum of 30% at high temperatures (> 750°C).

Phenomenological swelling equation – Lack of an expanded data base requires extrapolations from experimental data. To this end, a phenomenological swelling equation was developed (see ref. [4] for details):

$$\frac{\Delta V}{V} = \left(\frac{3}{4\pi}\right)^{1/2}\left[\left(\frac{kT}{2\gamma}\right)\left(\frac{f_R \dot{G}_{He} t}{N^{1/3}}\right)\right]^{3/2}, \qquad (1)$$

where k is the Boltzman's constant, T is temperature, γ is the surface tension, f_R is the fraction of retained helium gas, $\dot{G}_{He}$ is the helium generation rate, t is the time, and N is the bubble number density.

No measurements for the fraction of retained He atoms are reported. Therefore, for the purpose of using eq. (1), it is conservatively assumed that all He atoms produced during irradiation are trapped (f_R = 1). Beryllium surface-energy measurements have been performed and the values quoted range from 1 to 2 J/m^2 [65–68]. In calibrating eq. (1) to Beeston's data, a surface tension value of 1.6 J/m^2 leads to the best agreement between the model and the data. Table 5 shows a comparison of the experimental data [69] with predictions of eq. (1). For the temperature range between 300° and 500°C, good agreement between the model and measured swelling data is apparent.

Table 5
Experimental [a] and estimated [b] swelling values of beryllium

Temperature (°C)	$\Delta V/V$ (%)	
	Experiments [a]	Estimated [b]
200	1.2	0.36
300	1.5	1.29
400	3	3.17
500	6	6.69

[a] Specimen contained about 30,000 appm helium (3.7×10^{21} He/cm^3) [69].
[b] Estimated using eq. (1).

To estimate the swelling of the TITAN-II beryllium rods, it is assumed that high density Be, which retains most of the generated helium, is used. Table 6 shows the estimated Be swelling after one FPY of operation. The Be was assumed to have an average temperature of 500°C. It can be seen that with conservative assumptions, the maximum swelling should not be higher than ~ 15% at 0.5 cm behind the first wall.

A realistic model of beryllium swelling has to account for loss of helium through open pores and helium trapped in closed pores. Simple calculations were performed to estimate the fraction of helium released in the presence of open porosity [4] resulting in a fractional release value of 0.7 for a sphere-packed beryllium-bed at elevated 500°C. Based on this estimate for f_R and using eq. (1), the maximum Be swelling at 0.5 cm behind the first wall of TITAN-II is about 8.5%. These calculations assume that the pores in the beryllium rod remain open and do not sinter during operation (sintering must be minimized to avoid pore closure and excessive swelling). A smear density of

Table 6
Swelling of solid beryllium in the TITAN-II reactor [a]

Distance from first wall (cm)	Total Helium (appm)	$\Delta V/V$ (%)
0.5	53,400	14.5
4.9	34,000	7.4
9.5	20,300	3.4
14.5	11,900	1.5

[a] After 1 FPY of operation at 18 MW/m^2 neutron wall loading.

70% theoretical density (TD) can be achieved using sphere-packed Be. The maximum operating temperature must be kept below 660°C to prevent excessive sintering of the spheres. Beeston [70] has conducted experimental investigations of grain growth of beryllium that indicate open porosity below 661°C. The thermal conductivity of 70% TD beryllium at 600°C is about 44 W/m-°C [71].

Swelling limits – Extensive Be swelling will ultimately result in microcrack formation in the solid. Furthermore, at high helium generation rates and at elevated temperatures, a network of intelinking He bubbles can developed. These two mechanism are believed to limit swelling of Be to around 10%. However, these processes will also result in a reduction of the overall Be thermal conductivity. Localized hot spots could develop and cause sintering of Be and closure of open porosity or microcracks. Newly densified Be would then be again highly susceptible to He entrapment and consequently result in high localized swelling, which in turn would result in the above outlined microstructural changes. A cyclic process of closing and opening of porosity will ultimately lead to an equilibrium helium-venting rate with an associated maximum swelling value. Realistic temperature of the coolant is shown to be effective in reducing formation of decomposition products in non-boiling nuclear systems. More experimental data are required so that the radiolytic behavior of concentrated salt solutions can be predicated with a higher degree of confidence.

The low-activation ferritic alloy, 9-C, was chosen from among other reduced-activation ferritics because of its good strength and elongation behavior after irradiation. The high chromium content (11 wt%) of this alloy should provide good resistance to corrosion in an aqueous solution. The low-carbon content (0.09 wt%) reduces the risk of hydrogen embrittlement. Although no data on the ductile-to-brittle transition temperature (DBTT) is available, it is believed that the high manganese content (6.5 wt%) of 9-C will prevent the formation of delta-ferrite phases which are primarily responsible for increases of DBTT. The data base for corrosion of ferritics in $LiNO_3$ solutions is very limited. Indications are, however, that a high-concentration $LiNO_3$ solution does not exhibit unacceptable corrosion problems.

Hydrogen embrittlement of structural material is a major concern. The main influences are the hydrogen content and the temperature of the structural alloy. Reducing the amount of atomic hydrogen available for solution in the structure and operating at high temperatures are the most effective means of reducing hydrogen attack. Because atomic hydrogen is produced on metal surfaces during corrosion processes, minimizing corrosion also reduces hydrogen embrittlement. The production of tritium in the coolant does not necessarily result in an increased hydrogen attack since rapid recombination forms molecular hydrogen or water molecules. In fact, the Nelson curves, used by the petrochemical industry as guidelines, show that chromium steels can operate at 400°C with a hydrogen partial pressure of 17 MPa without experiencing hydrogen embrittlement [33].

Another form of attack on structural material exposed to aqueous solutions is stress-corrosion cracking. Most recent experiences with SCC in a nuclear environment clearly show that SCC can be suppressed by adding hydrogen which results in a reduction of the oxygen content. The production of tritium in an aqueous $LiNO_3$ solution is seen as an SCC-controlling mechanism. The proper choice of structural material can further reduce the probability of SCC. In particular, a high-chromium content coupled with a low-carbon content (as in the ferritic alloy, 9-C) are shown to reduce SCC.

The primary coolant contains 6.4 at.% lithium with a ^6Li enrichment of 12%. Estimated properties of this solution were used in the thermal-hydraulic calculations. Compared to water, this aqueous solution has a higher density, a lower specific heat capacity, and a higher boiling point. This implies that the thermal-hydraulic design of such an aqueous salt blanket will be different from that of a pure-water-cooled design. A lower coolant pressure or a higher operating temperature can be chosen.

The TITAN-II design requires a neutron multiplier to achieve an adequate tritium-breeding ratio. Beryllium is the primary neutron multiplier for the TITAN-II design. Investigation of the swelling behavior of Be shows the necessity of using either low-density, sphere-packed or high-density, fine-grained Be. Depending on the type chosen, different operating conditions must be satisfied to ensure minimum swelling and retention of structural integrity. Beryllium corrosion by an aqueous solution was also investigated. Past experience shows that minimizing carbonates, sulfates, and chlorates in solution reduces corrosion of Be. Coatings have also been developed and their effectiveness has been demonstrated. However, since most of the coatings were developed for radiation-free environments, research is needed to develop coatings that can withstand harsh radiation environments. For the TITAN-II design, a cladding of 9-C alloy surrounds the beryllium rods.

The engineering design study of the TITAN-II FPC indicates that this design is technically feasible. However, experimental investigations in several areas are needed to confirm the findings. Experimental measurements of the effects of corrosion, hydrogen embrittlement, and radiolysis in aqueous-coolant ferritic-steel systems are needed. Experimental data to confirm the estimated physical properties of nitrate solution, confirmation of the $LiNO_3$ subcooled-flow-boiling heat transfer, critical heat flux, and pressure drop are essential.

Acknowledgements

The TITAN research program is supported by the U.S. Department of Energy, Office of Fusion Energy, at University of California, Los Angeles under grant DE-FG03-86ER52126, at General Atomics under contract DE-AC03-84ER53158, at Rensselaer Polytechnic Institute under grant DE-FG02-85ER52118, and at Los Alamos National Laboratory which is operated by the University of California for the U.S. DOE under contract W-7405-ENG-36.

References

[1] F. Najmabadi, R.W. Conn, R. Krakowski, D. Steiner, K. Schultz, et al., Overview of the TITAN reversed-field-pinch fusion reactor study, Fusion Engrg. Des. 23 (1993) 69–80, in this issue.

[2] D. Steiner et al., A heavy water breeding blanket, in: Proc. 11th Symp. on Fusion Engineering, Austin, Texas (1985).

[3] S. Sharafat, N.M. Ghoniem, E. Cheng, P.I.H. Cooke, R. Martin, F. Najmabadi, and C.P.C. Wong, TITAN-I fusion-power-core materials engineering and design considerations, Fusion Engrg. Des. 23 (1993) 99–113, in this issue.

[4] F. Najmabadi, R.W. Conn, R. Krakowski, D. Steiner, K. Schultz, et al., The TITAN reversed-field pinch fusion reactor study; the Final Report, joint report of University of California Los Angeles, General Atomics, Los Alamos National Laboratory, and Rensselaer Polytechnic Institute, UCLA-PPG-1200 (1990).

[5] J.T. Kiwi and M. Daniels, On the radiolysis of concentrated alkaline and calcium-nitrate solutions, J. Inorg. Nucl. Chem. 40 (1978) 576.

[6] M. Daniels, Radiolysis and photolysis of the aqueous nitrate system, in: Radiation Chemistry, Vol. 1, R.F. Gould (Ed.), American Nuclear Society, Washington D.C. (1968).

[7] M. Burton and K.C. Kurien, Effects of solute concentration in radiolysis of water, J. Phys. Chem. 63 (1959) 899.

[8] H.A. Schwarz, The effect of solutes on the molecular yields in the radiolysis of aqueous solutions, J. Am. Chem. Soc. 77 (1955) 4960.

[9] J.A. Lane, H.G. MacPherson, and F. Maslan, Fluid fuel reactors, in: Atoms for Peace (Addison-Wesley Publishing Company, Inc., New York, 1958).

[10] R.G. Sowden, The effect of nitrate ion on the yield of hydrogen from water radiolysis, J. Am. Chem. Soc. 79 (1957) 1263.

[11] W.G. Burns and P.B. Moore, The radiation chemistry of high temperature (300–400°C) water, Harwell Laboratory report AERE-R9516, England (1980).

[12] P. Cohen, Water coolant technology of power reactors, American Nuclear Society (1980).

[13] T. Kambara, R.M. Whites, and F.S. Rowland, The reactions of recoil tritium atoms in aqueous solution, J. Inorg. Nucl. Chem. 21 (1961) 210.

[14] D.S. Gelles, N.M. Ghoniem, and R.W. Powell, Low activation ferritic alloys patent description, University of California Los Angeles report UCLA/ENG-87-9/PPG-1049 (1987).

[15] R.L. Klueh, D.S. Gelles, and T.A. Lechtenberg, Development of ferritic steels for reduced activation: the U.S. program, J. Nucl. Mater. 141–143 (1986) 1081.

[16] J.M. Vitek and R.L. Klueh, Alloy development for irradiation performance, ADIP Semiannual Progress Report, U.S. Department of Energy report DOE/ER-0045/12 (March 31, 1984) 110.

[17] T.A. Lechtenberg, General Atomics, San Diego, CA, private communication (March 1987).

[18] D.N. Braski, The effect of neutron irradiation on the tensile properties and microstructure of several vanadium alloys, in: Proc. ASTM Conf. on Fusion Reactor Materials, Seattle, WA (1986).

[19] B. Craig, Hydrogen damage in: Metals Handbook, 9th edition 13 (1987) 163.

[20] G. Sandoz, A unified theory for some effects of hydrogen source, alloying elements and potential on crack growth in martensitic AISI 4330 steel, Metall. Trans. 3 (1972) 213.

[21] A.B. Bond and H.J. Dundas, Stress corrosion cracking of ferritic stainless steels, in: Proc. of Stress Corrosion Cracking and Hydrogen Embrittlement of Iron Base Alloys, R.W. Staehle, J. Hochmann, R.D. McCright, and J.E. Slate (Eds.), Unieux-Firminy, France, June 12–16, 1973) 1136.

[22] D.H. Zhon, W.X. Zhon, and Z.L. Xu, Hydrogen degradation of 21-6-9 and medium carbon steels by disk-pressure test, J. Nucl. Mater. 141–143 (1986) 503.

[23] H.R. Gray, Testing for hydrogen environment embrittlement: experimental variables, in: Hydrogen Embrittlement Testing, American Society for Testing and Materials (ASTM STP 543), Philadelphia (1974) p. 133.

[24] J.P. Fidelle, R. Borudeur, C. Rowx, and M. Rapin, Disk pressure testing of hydrogen environment embrittlement, in: Hydrogen Embrittlement Testing, American Society for Testing and Materials (ASTM STP 543), Philadelphia (1974) p. 221.

[25] W.T. Chandler and R.J. Walter, Testing to determine the effect of high-pressure hydrogen environments on the mechanical properties of metals, in Hydrogen Embrittlement Testing, American Society for Testing and Materials (ASTM STP 543), Philadelphia (1974) p. 171.
[26] B.A. Graville, R.G. Baker, and F. Watkinson, Br. Weld J. 14 (1967) 337.
[27] J.B. Lee, A.K. Agrawald, and R.W. Staehle, Corrosion and corrosion cracking of materials for water-cooled reactors, Electric Power Research Institute (EPRI) report NP-1741 (1981).
[28] L.G. Ljungberg, D. Cubicciotti, and M. Trolle, Material behavior in alternate (hydrogenated) water chemistry in the Ringhals-1 boiling water reactor, Corrosion 42 (1986) 263.
[29] B.M. Gordon, W.L. Clarke, M.E. Indig, A.E. Pickett, and M.T. Wang, Corrosion/81, Paper No. 20, National Association of Corrosion Engineers, Houston, TX (1981).
[30] R.L. Gowan et al., Assessment of operation of the Dresden-2 nuclear power station under hydrogen water chemistry, prepared by General Electric for Nuclear Energy Business Operation (July 1984).
[31] B.M. Gordon, C.W. Jewett, A.E. Pickett, and M.E. Indig, Corrosion resistance improvement of ferritic steels through the hydrogen addition to the BWR coolant, Proc. of Topical Conference on Ferritic Alloys for Use in Nuclear Energy Technologies, AIME, Snowbird, UT, June 19–23, 1983, 65.
[32] Steels for hydrogen service at elevated temperatures and pressures in petroleum refineries and petrochemical plants, API Publication 941, 2nd edition (1971).
[33] R.S. Treseder, Guarding against hydrogen embrittlement, Chem. Engrg. 29 (1981) 105.
[34] M.G. Fontana and N.D. Greene, Corrosion Engineering (McGraw-Hill International Book Company, Singapore, 1978).
[35] J.C. Danko, Corrosion in the nuclear power industry, in: Metals Handbook, 9th edition, 13 (1987) 927.
[36] A. McNinn, Stress corrosion of high-chromium nickel-base metals and AISI 316 nuclear grade stainless steel in simulated boiler water reactor environment, Corrosion 42 (1986) 682.
[37] R.N. Parkins, Environmental aspects of stress corrosion cracking in low strength ferritic steels, in: Proc. of Stress Corrosion Cracking and Hydrogen Embrittlement of Iron Base Alloys, R.W. Staehle, J. Hochmann, R.D. McCright, and J.E. Slate (Eds.), Unieux-Firminy, France (June 12–16, 1973) 601.
[38] R. Waeben, W. Bogaert, and M. Embrecht, Initial corrosion evaluation of candidate materials for an ASCB driver blanket for NET, Proc. IEEE 12th Symp. Fusion Engineering, Monterey, CA (October 12–16, 1987) 1332.
[39] W.F. Bogaerts, M.J. Embrechts, and R. Waeben, Application of the aqueous self-cooled blanket concept to a tritium producing shielding blanket for NET, University of Leuven (Belgium) report EUR-FU/XII-80/87/75 (1987).
[40] P.L. Andresen, The effects of aqueous impurities on IGSCC of sensitized type 304 stainless steel, Electric Power Research Institute (EPRI) report NP-3384 (1983).
[41] R.N. Parkins and R. Usher, Proc. 1st Int. Congr. Metallic Corrosion (Butterworths, London, 1961) p. 289.
[42] Z. Szklarska-Smialowska, Effect of potential of mild steel on stress corrosion cracking in ammonium nitrate solutions, Corrosion 20 (1964) 198.
[43] W. Radeker and H. Grafen, Stahl und Eisen 76 (1956) 1616.
[44] H. Mazille and H.H. Uhlig, Effect of temperature and some inhibitors on stress corrosion cracking of carbon steels in nitrate and alkaline solutions, Corrosion 28 (1972) 427.
[45] R.H. Wood, University of Delaware, Newark, personal communication (August 1987).
[46] L.V. Puchkov and V.G. Matashkin, Densities of $LiNO_3$-H_2O and $NaNO_3$-H_2O solutions at temperatures in the range 25–300°C, J. App. Chem. USSR 43 (1970) 1864.
[47] L.V. Puchkov, V.G. Matashkin, and R.P. Matveeva, Density of aqueous lithium nitrate solutions at high temperatures (up to 350°C) and concentrations, J. App. Chem. USSR 52 (1979) 1167.
[48] L.V. Puchkov and P.M. Sargaev, Viscosities of lithium, sodium, potassium, and ammonium nitrate solutions at temperatures up to 275°C, J. App. Chem. USSR 46 (1973) 2367.
[49] L.V. Puchkov and P.M. Sargaev, Dependence of viscosity of electrolyte solutions on temperature and concentration, J. App. Chem. USSR 47 (1974) 280.
[50] R.H. Wood and J.R. Quint, A relation between the critical properties of aqueous salt solutions and the heat capacity of the solutions near the critical point using a single-fluid corresponding-states theory, J. Chem. Thermodynamics 14 (1982) 14.
[51] W.L. Marshall and E.V. Jones, Liquid-vapor critical temperatures of aqueous electrolyte solutions, J. Inorg. Nucl. Chem. 36 (1974) 2313.
[52] S. Sourirajan and G.C. Kennedy, The system H_2O–NaCl at elevated temperatures and pressures, Am. J. Sci. 260 (1962) 115.
[53] H. Ozbek and S.L. Phillips, Thermal conductivity of aqueous sodium chloride solutions from 20 to 330°C, J. Chem. Eng. Data 25 (1980) 263.
[54] G.A. Sacchetto, G.G. Bombi, and C. Macca, Vapor pressure of very concentrated electrolyte solutions, J. Chem. Thermodynamics 13 (1981) 31.
[55] D. Webster and G.J. London (Eds.), Beryllium Science and Technology (Plenum Press, New York and London, 1979).
[56] J.N. Wanklyn and P.J. Jones, The aqueous corrosion of reactor metals, J. Nucl. Mater. 63 (1962) 291.
[57] A.J. Stonehouse and W.W. Beaver, Beryllium corrosion and how to prevent it, Mater. Prot. 4 (1965) 24.
[58] P.D. Miller and W.K. Boyd, Beryllium deters corrosion–Some do's and don'ts, Mater. Engrg. 68 (1968) 33.
[59] J. Brooker and A.J. Stonehouse, Chemical conversion coatings retard corrosion of beryllium, Mater. Prot. 8 (1969) 43.

[60] J.B. Rich and G.P. Walters, The effects of heating neutron irradiated beryllium, J. Nucl. Mater. 1 (1959) 96.
[61] C.E. Ells and E.C.W. Perryman, Effects of neutron-induced gas formation on beryllium, J. Nucl. Mater. 1 (1959) 73.
[62] J.R. Weir, The effects of high-temperature reactor irradiation on some physical and mechanical properties of beryllium, Proc. of Int. Conf. Metallurgy of Beryllium, Institute of Metals, London (October 1961) 362.
[63] J.B. Rich and R.S. Barnes, Mechanical properties of some highly irradiated beryllium, J. Nucl. Mater. 4 (1961) 287.
[64] M.O. Tucker and R.J. White, The geometry in interlinked grain edge porosity, Res Mechanica 1 (1980) 21.
[65] R.S. Barnes and G.B. Redding, Neutron lifetime measurement in the fast reactors Zeus and Zephyr, Nucl. Energy 10 (1959) 22.
[66] J.B. Rich, The mechanical properties of beryllium irradiated at 350 and 600°C, in: The Metallurgy of Beryllium (Institute of Metals, Chapman and Hall, Ltd., London, 1963) p. 135.
[67] L.E. Muir, Interfacial Phenomena in Metals and Alloys (Addison-Wesley Publishing Corp., Reading, MA, 1975) p. 124.
[68] W.G. Wolfer and T.J. McGarville, Swelling of beryllium, in: Damage Analysis and Fundamental Studies, U.S. Department of Energy report DOE/ER-0046/19 (November 1984).
[69] J.M. Beeston, L.G. Miller, E.L. Wood, and R.W. Moir, Comparison of compression properties and swelling of beryllium irradiated at various temperatures, Idaho National Engineering Laboratory report EGG-FT-6608 (1984).
[70] J.M. Beeston, Gas release and compression properties in beryllium irradiated at 600 and 700°C, in: Effects of Irradiation on Structural Metals, American Society of Testing and Materials (ASTM STP 426) (1967) 135.
[71] G.P. Marino, The porosity correction factor for the thermal conductivity of ceramic fuels, J. Nucl. Mater. 38 (1971) 178.